High-pressure Raman study of the ferroelastic rutile-to-$CaCl_2$ phase transition in ZnF_2

Aristides Perakis, Dimitrios Lampakis, Yannis C. Boulmetis, and Constantine Raptis
Department of Physics, National Technical University of Athens, GR-15780 Athens, Greece
(Received 26 April 2005; revised manuscript received 24 August 2005; published 24 October 2005)

The high-pressure Raman spectra of ZnF_2 have been measured up to 6.8 GPa and provided unambiguous evidence of a phase transition from its ambient-pressure rutile (D_{4h}^{14}) to the $CaCl_2$-type orthorhombic (D_{2h}^{12}) structure at a pressure $P_c \approx 4.5$ GPa. Both macro- and micro-Raman spectra have been independently obtained at high pressures leading to the same conclusion about the high-pressure phase and the P_c. The transition appears to be closely associated with the B_{1g} (A_g) Raman-active *soft mode* of the rutile ($CaCl_2$) structure, implying that ZnF_2 undergoes a second-order ferroelastic phase transition.

DOI: 10.1103/PhysRevB.72.144108 PACS number(s): 64.70.Kb, 78.30.Hv, 61.50.Ks, 63.20.−e

I. INTRODUCTION

A characteristic feature in the Raman spectra of tetragonal rutile-type crystals, space group D_{4h}^{14}, is the anomalous temperature and pressure dependence of the B_{1g} soft mode which softens with either *decreasing* temperature[1–6] or *increasing* pressure.[1,7–12] The anomalous, nonlinear B_{1g} mode softening with temperature could be considered as a precursor for an incoming phase transition of these crystals at low temperatures. Lockwood *et al.*[3] and recently Perakis and co-workers[6,13] have reported that the B_{1g} softening with decreasing temperature in the rutile-structured FeF_2 (Ref. 3), MgF_2 (Ref. 6), and ZnF_2 and MnF_2 (Ref. 13) is primarily due to thermal contraction and concluded[3,6,13] that, if any structural change is involved, it would be incomplete. So far, there have been no reports of any rutile-type crystal (at ambient conditions) undergoing a definite low-temperature phase transition. However, the rutile-to-$CaCl_2$-structure (space group D_{2h}^{12}) phase transition has been observed at high temperatures in x-ray[14] and Raman[15,16] studies of $CaBr_2$ and $CaCl_2$, which are orthorhombic at ambient conditions.

Pascual *et al.*[10] observed a linear dependence of the B_{1g} mode softening in MgF_2 under uniaxial stress. This result may be interpreted that the pressure induced B_{1g} softening is not also associated with a definite structural change. It must be pointed out, though, that the range of applied stresses in that study[10] was limited up to a fraction of a GPa. On the whole, the anomalous B_{1g} mode softening with pressure of rutile-type crystals has been associated, in early[1,7–9] and recent[11,12,17,18] reports, with an incipient phase transition. There have been different propositions concerning the high-pressure phase of these crystals, varying from orthorhombic α-PbO_2 (Refs. 7 and 17), cubic fluorite[19] or modified cubic fluorite[18] and orthorhombic $CaCl_2$ type (Refs. 8, 11, 12, 20, and 21). In fact, the variety of views about the high-pressure phase of rutlile-type crystals reflects the rather complex sequence[20,21] of high-pressure transitions in which different phases may co-exist at a given pressure.[21]

Recent Raman studies by Haines *et al.*[11] and Hellwig *et al.*,[12] and x-ray studies by Haines and co-workers[20,21] point out that the *first high-pressure* transition in most rutile-structured dioxides, such as SnO_2, GeO_2, PbO_2, MnO_2, etc, as well as in MgF_2, is to the $CaCl_2$-type structure. Also, it has been reported in x-ray[22] and Raman[23] studies that the rutile-structured polymorph of SiO_2 (stishovite) sustains a transition to the $CaCl_2$-type structure at high pressure. Most of the high-pressure studies on rutile-type crystals refer to dioxides. In contrast, the rutile-structured difluorides have not had the same attention. Moreover, with the exception of the uniaxial stress study on MgF_2 (Ref. 10), there have not been any high-pressure Raman works related to rutile-type difluorides, most likely because of their very low Raman-scattering efficiencies which result in particularly low Raman signals from the high-pressure cell.

ZnF_2 is a rutile-structured difluoride at ambient conditions whose Raman spectrum has been studied at room[24] and low[4] temperatures, but not at high pressures. In this work, we present macro- and micro-Raman-scattering measurements from single crystals of ZnF_2 at high pressures and report a definite first phase transition to the $CaCl_2$-type structure at about 4.5 GPa. From the correlation of Raman modes between the rutile and $CaCl_2$-type structures, it is implied that the transition is mediated by the lowest-frequency B_{1g} (A_g) mode of the rutile ($CaCl_2$) structure, which displays soft mode behavior.

II. EXPERIMENTAL DETAILS

Two different diamond anvil cells (DAC) were used for the room temperature high-pressure Raman experiments: a Syassen-Holzapfel–type for the macro-Raman measurements and a Merril-Basset for the micro-Raman ones. In either case, the back-scattered (micro-Raman) or nearly back-scattered (macro-Raman) light from the DAC was analyzed and detected by a system of a T 64000 model Jobin-Yvon triple spectrometer, operated in subtractive mode, in conjunction with a nitrogen cooled charge coupled device (CCD). For the micro-Raman measurements, the spectrometer was combined with a $\times 40$ magnification lens. We have recorded macro-Raman spectra up to 5.1 GPa; above this pressure, the intense background scattering (especially in the lower part of the spectrum) prevented a reliable assessment of the Raman peaks of ZnF_2. As for the micro-Raman measurements, we have practically covered the entire pressure range of operation for the corresponding DAC.

Small chips of ZnF_2 (cut from a larger single crystal) were loaded into the high-pressure cells in which a 4:1 methanol-ethanol mixture was used as pressure transmitting medium. Measurement of pressure inside the DAC was achieved via the (well-known) pressure-induced shift of the Raman-active optical phonon of a silicon crystal chip placed alongside the ZnF_2 chip. The macro-Raman spectra were calibrated with the use of spectral lines of an argon lamp (or the Raman lines of the DAC sapphire windows). For the micro-Raman measurements, the spectrometer was calibrated prior to each high-pressure experiment, by recording separately outside the DAC the ambient pressure Raman spectrum of a silicon single crystal; for best accuracy, this crystal and the silicon chip inside the DAC were pieces cut from the same larger silicon single crystal.

The Raman spectra were excited by the 514.5 nm line of an Ar^+ laser at a power of ~150 and ~3 mW (at the entrance of the high-pressure cell) for the macro- and the micro-experiments, respectively.

The macro-Raman spectra were not polarized as no analyzer was placed in the path of the scattered beam. This was primarily imposed by the very weak scattered signal obtained from the macro-Raman setup; thus, in the recorded macro-Raman spectra of ZnF_2 (see Sec. III) the intensities of the two observed phonons, A_{1g} (corresponding to diagonal components of the Raman tensor) and E_g (nondiagonal components of the Raman tensor) are comparable. On the other hand, in order to observe the splitting of the E_g mode at high pressures, polarized micro-Raman spectra were obtained, in successive recordings, by rotating at 90° a linear polarizer which was appropriately located at square angle to the exciting beam path. In this way, Raman spectra in the backscattering configurations (i) $z(xx)\bar{z}$ or (ii) $z(yx)\bar{z}$ have been obtained in which the directions and polarizations of incident and scattered beams (represented by the symbols outside and inside the notation, respectively) refer to the laboratory frame axes x, y, z and not to the crystallographic axes of the ZnF_2 crystal as the orientation of the latter is not known inside the DAC. Strictly speaking, as a consequence of the unknown crystal orientation inside the DAC, polarization selection rules for the identification of symmetries of Raman modes cannot be applied for high-pressure Raman measurements; however, as the scattering configurations $z(xx)\bar{z}$ and $z(yx)\bar{z}$ favor the observation of diagonal and nondiagonal elements of the Raman tensor, respectively, we have used in certain occasions, these polarized configurations in order to selectively enhance the A_{1g} or the E_g Raman mode of ZnF_2.

III. RESULTS AND DISCUSSION

Macro- and micro-Raman spectra of ZnF_2 at various pressures are shown in Figs. 1 and 2, respectively. All spectra in these figures were recorded with the sample inside the respective DAC, except the ambient-pressure micro-Raman one, with the vertically enlarged B_{1g} and B_{2g} modes (insets), at the bottom of Fig. 2, which was recorded separately using a larger crystal outside the DAC. The frequencies of the four Raman-active phonons of ZnF_2 at ambient-conditions are 69 (B_{1g}), 248 (E_g), 347 (A_{1g}), and 523 cm^{-1} (B_{2g}). In the macro-Raman spectra (Fig. 1), apart from the Raman peaks of ZnF_2 and that of the silicon chip (at about 521 cm^{-1}), some Raman lines due to the sapphire windows of the DAC are also observed at 378 and 418 cm^{-1}. In the low-pressure macro-Raman measurements, the argon lamp calibration lines at 64.5, 159.7, 283.7, and 397 cm^{-1} have been recorded in the same scan and are present in the corresponding spectra of Fig. 1. At higher pressures, as the E_g and A_{1g} phonon peaks shift to higher frequencies and overlap with the above argon lines, the argon lamp is not used for calibration; in such cases, the sapphire Raman lines are used for calibration of spectra.

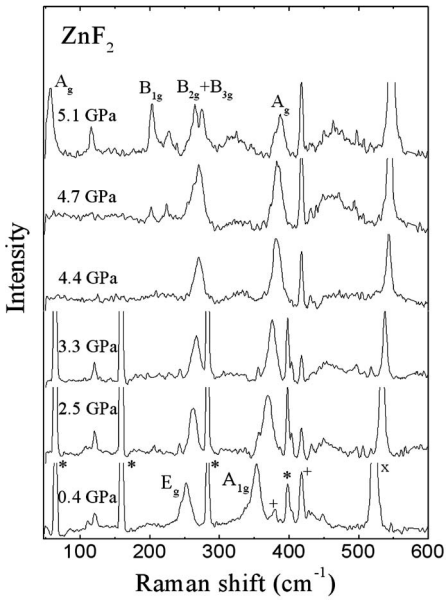

FIG. 1. Unpolarized macro-Raman spectra of ZnF_2 at various pressures. Two Raman peaks are observed in the low-pressure (rutile-type) phase and five in the high-pressure ($CaCl_2$-type) one. *, Argon lamp calibration lines; +, Raman lines of the sapphire window of the high-pressure cell; ×, pressure monitoring Raman line of a Si chip (placed inside the high-pressure cell).

In the micro-Raman spectra of Fig. 2, a noticeable variation with pressure of the relative intensity between the E_g and A_{1g} modes is primarily due to the different polarization configurations $z(xx)\bar{z}$ or $z(yx)\bar{z}$, which relatively enhance (supress) the A_{1g} (E_g) or the E_g (A_{1g}) phonons, respectively (see Sec. II for details). In addition, this variation may be partly owed to the reorientation of the sample inside the DAC upon increasing the applied pressure, or/and to rotation of the DAC and sample around the direction of the exciting laser beam; such a rotation is possible only in the micro-Raman setup and has been performed in order to detect the splitting of the E_g mode at pressures above 4.5 GPa (see relevant analysis and discussion below).

At low pressures, only the A_{1g} and E_g modes of the rutile phase of ZnF_2 were observed from the DAC. It was not possible to observe the B_{1g} and B_{2g} modes of the rutile phase from either high-pressure setup, because of their extremely weak intensity (see lower spectrum of Fig. 2). It is obvious from Figs. 1 and 2 that the A_{1g} and E_g modes display normal-mode behavior with pressure, that is, they harden with in-

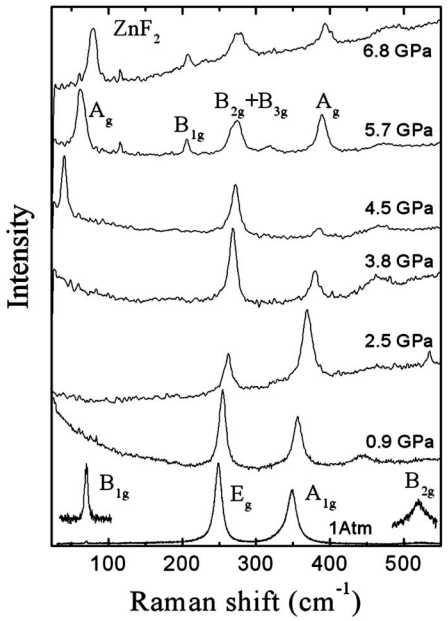

FIG. 2. Micro-Raman spectra of ZnF_2 at various pressures. The spectra at ambient pressure and at pressures 0.9, 5.7, and 6.8 GPa are unpolarized (without an analyzer in the path of the scattered beam); the spectrum at 2.5 GPa is polarized with the scattering configuration $z(xx)\bar{z}$, giving a relatively enhanced A_{1g} phonon, which corresponds to diagonal elements of the Raman tensor; the spectra at 3.8 and 4.5 GPa are cross-polarized corresponding to the scattering configuration $z(yx)\bar{z}$, which relatively elevates the nondiagonal E_g phonon (see text for details). In the ambient-pressure spectrum, the sample was outside the high-pressure cell; the weak B_{1g} and B_{2g} phonon lines of this spectrum have been vertically enlarged and shown as insets. Two Raman peaks are observed in the low-pressure (rutile) phase and four in the high-pressure ($CaCl_2$-type) structure, with one of the latter peaks being double corresponding to the unresolved B_{2g} and B_{3g} modes.

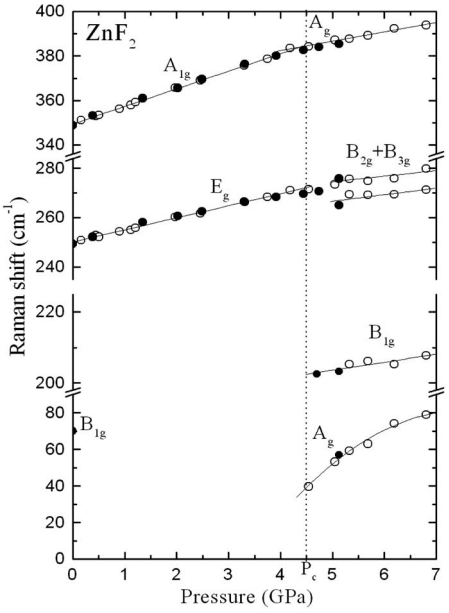

FIG. 3. Raman mode frequencies of ZnF_2 plotted against pressure. Solid circles correspond to macro-Raman measurements and open circles to micro-Raman ones. All modes display linear dependence, except the A_g symmetry one of the high-pressure phase which shows nonlinear, soft mode behavior. Note the change of slope of the $A_{1g}(\rightarrow A_g)$ and the splitting of the $E_g(\rightarrow B_{2g}+B_{3g})$ modes of the low-frequency phase at ~4.5 GPa.

creasing pressure. This effect is illustrated in Fig. 3 which shows plots of mode frequencies with pressure. From the, almost, linear dependence of $\omega(A_{1g})$ and $\omega(E_g)$ with pressure (Fig. 3), Grüneisen parameters $\gamma_T=(B/\omega_0)/(\partial\omega/\partial P)$ have been evaluated for these modes, where $B(=1/\kappa)$ is the bulk modulus (κ, the volume compressibility) and ω_0 the mode frequency at ambient conditions; in these calculations we have used the measured bulk modulus data for ZnF_2 of Gerlich *et al.*[25] In the absence of previous relevant experimental data, we compare our gamma values with theoretical ones based on a rigid ion model with a Born-type potential for nearest-neighbor interactions;[26,27] in the model of Ref. 27, long-range interactions are also included. The γ values of this work and the calculated ones[26,27] are summarized in Table I, showing better agreement of our data with those of Ref. 27. This agreement indicates that Coulomb interactions may play a significant part in the nature of the atomic bonding in ZnF_2 and is compatible with the conclusion drawn in a very recent near-edge x-ray-absorption fine structure study[28] that ZnF_2 is the most ionic among a number of rutile-structured difluorides, such as MnF_2, FeF_2, CoF_2, and NiF_2. In Table I, the calculated[26,27] Grüneisen parameters for the other two B_{1g} and B_{2g} modes are also included, showing a negative value for the former phonon.

At about 4.5 GPa, significant changes are observed in both macro- and micro-Raman spectra of ZnF_2, including a decrease of slope in the frequency-pressure plot of the A_{1g} mode (Fig. 3), a broadening and eventual splitting of the doubly degenerate E_g mode, and the appearance of two additional Raman lines above this pressure. As will be discussed below, these spectral changes imply unambiguously the onset of a structural phase transition in ZnF_2 at this pressure from tetragonal (D_{4h}^{14}) rutile-type to orthorhombic (D_{2h}^{12}) $CaCl_2$-type structure.

Prior to a detailed discussion on the evolution of the Raman-active modes of the tetragonal rutile-type phase of ZnF_2 and on the consequent mode assignment of the high-pressure phase, we discuss briefly some group theory compatibility aspects between the two crystal classes, that is between the tetragonal and the, most likely, orthorhombic phase at high pressures. The tetragonal D_{4h}^{14} rutile-type crystals have a bimolecular unit cell. The Brillouin-zone-center optical modes of this crystal class have the irreducible representation:[12,15]

$$A_{1g}+E_g+B_{1g}+B_{2g}+A_{2g}+A_{2u}+3E_u+2B_{1u},$$

where A_{1g}, E_g, B_{1g}, and B_{2g} are Raman-active modes and the E-symmetry species are twofold degenerate. The orthorhombic D_{2h}^{12} $CaCl_2$-structure has also a bimolecular unit cell and the irreducible representation of the zone-center optical modes for this structure is[12,15]

TABLE I. Mode Grüneisen γ_T parameters of ZnF_2 for both the low-pressure rutile-type and the high-pressure $CaCl_2$-type structures.

Rutile-type structure					$CaCl_2$-type structure	
Mode-symmetry	This work	Ref. 26	Ref. 27		Mode-symmetry	This work
A_{1g}	2.30[a]	1.62[b]	2.70[b]	↔	A_g	1.31[c]
B_{1g}	—	−5.66[b]	−8.10[b]	↔	A_g	72.50[c] 17.50[d]
B_{2g}	—	1.43[b]	1.50[b]	↔	B_{1g}	—
E_g	2.05[a]	2.35[b]	2.40[b]	↔	B_{2g}	1.00[c]
					B_{3g}	1.05[c]
					B_{1g}	1.05[c,e]

[a]Gamma values corresponding to experimental $\partial\omega/\partial P$ slopes and ω_0 frequencies at ambient conditions obtained in this work.
[b]Theoretical values.
[c]Values corresponding to experimental $\partial\omega/\partial P$ slopes and ω_0 frequencies at ~4.5 GPa obtained in this work, and assuming a bulk modulus B value equal to that at ambient pressure (Ref. 25).
[d]Gamma value of the A_g soft mode of the high-pressure phase at 6.8 GPa.
[e]Gamma value for the new B_{1g} Raman mode of the high-pressure phase which originates from the A_{2g} Raman-inactive mode of the low-pressure phase.

$$2A_g + 2B_{1g} + B_{2g} + B_{3g} + 2A_u + B_{1u} + 3B_{2u} + 3B_{3u},$$

with A_g, B_{1g}, B_{2g}, and B_{3g} being the Raman-active species. According to group theory, the orthorhombic D_{2h}^{12} space group is a direct subgroup of the tetragonal (rutile) D_{4h}^{14} group, so that the two irreducible representations are compatible giving direct mode correlations[12,15] for the rutile-to-$CaCl_2$-type structure transition.

The broadening of the E_g mode above the critical pressure P_c=4.5 GPa can be realized directly by examining the evolution of the spectra of Figs. 1 and 2. This result has been confirmed by measuring in succession two cross-polarized $z(yx)\bar{z}$ micro-Raman spectra at the same pressure above 4.5 GPa, but with different sample orientation. Figure 4 shows in detail the E_g mode line at four pressures between 4.5 and 6.8 GPa recorded with the micro-Raman setup. In all the spectra of Fig. 4, the $z(yx)\bar{z}$ scattering configuration was used that favors nondiagonal elements of the Raman tensor (see Sec. II). The dual spectra at each of the pressures 5.7 and 6.2 GPa were recorded in succession under the same conditions, except for the orientation of the ZnF_2 crystal which was relatively rotated at 90° following a likewise rotation of the DAC around the direction of the incident beam. On the other hand, the single spectra at 4.5 and 6.8 GPa were recorded with the DAC orientation at mid position (45° rotation). It is obvious from the dual spectra of Fig. 4 that the E_g mode becomes a double peak line above P_c. The two peaks are not completely resolved in the micro-Raman spectra, but the full width at half maximum (FWHM) of the line increases abruptly above P_c, as the inset of Fig. 4 indicates; the FWHM values in this inset correspond to micro-Raman data. From the same inset, it can be seen that the respective FWHM plot for the A_{1g} mode is practically pressure-independent for the entire pressure range. Therefore, the E_g mode broadening and eventual splitting cannot be attributed

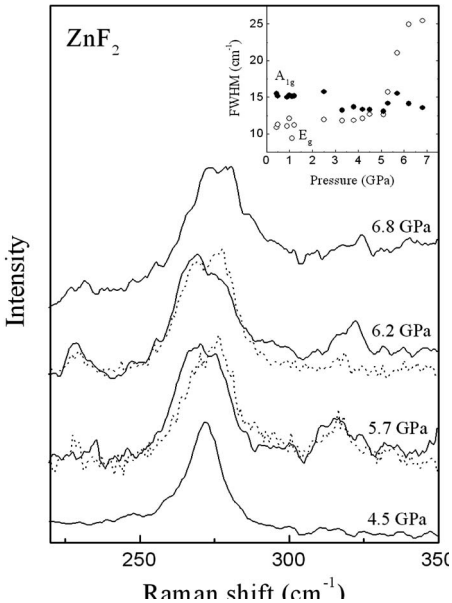

FIG. 4. Cross-polarized $z(xx)\bar{z}$ micro-Raman spectra of ZnF_2 showing that the doubly degenerate E_g mode of the low-pressure phase evolves into a double peak at high pressures. The dual spectra at each of the pressures 5.7 and 6.2 GPa correspond to two orientations of the ZnF_2 crystal sample differing by 90° with respect to the direction of the incident laser beam (see text for details), confirming that this line is a double peak spectral feature; the single spectra at 4.5 and 6.8 GPa correspond to the mid-position orientation of the sample, i.e. rotation of the DAC and sample at 45° relatively to either of the two extreme orientations. The inset shows plots for the full width at half-maximum (FWHM) of the $A_{1g}(A_g)$ and $E_g(B_{2g}+B_{3g})$ modes of the low- (high-) pressure phase; a sharp increase of the E_g mode width is observed at ~5.0 GPa, indicating the onset of splitting of this mode.

to nonhydrostatic pressure (stress) effects. Further evidence is provided by the macro-Raman spectrum at 5.1 GPa (Fig. 1) in which a definite splitting of the E_g mode is observed.

From the above, it is evident that the doubly degenerate E_g Raman mode of the rutile phase splits to two peaks above P_c which implies, according to group theory operations, an orthorhombic distortion of the rutile unit cell. In the event the high-pressure phase of ZnF_2 has the orthorhombic (D_{2h}^{12}) $CaCl_2$-type structure, the E_g phonon should transform to two phonon species of B_{2g} and B_{3g} symmetries according to group theory mode compatibilities.[12,15] Note that there is a decrease of slope for the (assumed) B_{2g} and B_{3g} modes in the frequency-pressure plots (Fig. 3) in relation to the E_g low-pressure phase mode.

Further study of the evolution of spectra in Figs. 1 and 2 reveals the appearance of two new Raman lines from ZnF_2 at about and above P_c. The lower frequency one is observed first in the micro-Raman spectra at exactly the critical pressure P_c=4.5 GPa and at a frequency of 40 cm^{-1}; above P_c, its frequency increases rapidly and nonlinearly with pressure (Fig. 3), thus showing characteristics of a soft mode. Plotting the squared frequency (ω^2) of this line against pressure reveals an almost linear dependence. This high-pressure line of ZnF_2 is assigned as the A_g symmetry mode of the orthorhombic phase and all the available evidence indicates that it is the counterpart of the B_{1g} soft mode of the rutile phase (see, also, mode correlation in Refs. 12 and 15). Although it has not been possible to observe the very weak B_{1g} mode of the rutile phase from the DAC and there are no relevant Raman data available for any rutile-structured fluorides, we think that this mode of ZnF_2 would display soft mode behavior with pressure like the rutile-structured oxides GeO_2 (Ref. 11) and SnO_2 (Ref. 12). This is reasonable bearing in mind the negative theoretical Grüneisen parameters[26,27] for this mode and the softening of the shear elastic constant $(C_{11}\text{-}C_{12})/2$ of ZnF_2 with pressure.[29] It is pointed out that this elastic constant describes[12,30] the transverse acoustic mode propagating along the {110} direction (in the *a*-*b* plane) and is coupled[3] with the rotational atomic displacements which correspond to the B_{1g} optical mode of rutile-type crystals. Hence, the high-pressure soft mode of ZnF_2 should be considered as the successor of the B_{1g} mode of the low-pressure rutile phase and, keeping in mind the mode correlation,[12,15] it is assigned as a A_g symmetry mode of the (D_{2h}^{12}) $CaCl_2$-type structure. Also, this soft mode is just observed at the edge (58 cm^{-1}) of the highest-attainable-pressure (5.1 GPa) macro-Raman spectrum (Fig. 1).

The second new Raman line of ZnF_2 above P_c is observed at about 203 cm^{-1} (macro: 4.7 GPa) and 205 cm^{-1} (micro: 5.3 GPa). This line hardens linearly with pressure (Fig. 3) and seems to become gradually stronger with increasing pressure, implying that it originates from a Raman-silent mode of the low-pressure rutile structure. As the only Raman-silent mode of the low-pressure phase which can be Raman-active in a tetragonal to orthorhombic transition is the A_{2g} symmetry one, then the corresponding high-pressure mode should be of B_{1g} symmetry (see mode correlation table of Refs. 12 and 15) if a transition from D_{4h}^{14} to D_{2h}^{12} structure were to occur. The mode correlation for such a transition[12,15] shows that the orthorhombic phase has six Raman-active modes, that is, two more than the rutile phase which result from the splitting of the E_g mode to B_{2g} and B_{3g} ones, and the activation of the A_{2g} mode becoming B_{1g} active in the lower-symmetry phase. In the high-pressure phase of ZnF_2 we observe five Raman phonons that are readily correlated to the low-pressure phase phonons according to the mode compatibility for the $D_{4h} \rightarrow D_{2h}$ transition; the sixth phonon of B_{1g} symmetry anticipated in the high-pressure phase has not been observed, implying that, like the original B_{2g} phonon of the tetragonal phase, it is very weak for detection from the DAC. It must be pointed out that Raman scattering alone is not often in a position to identify unambiguously the space group of crystals, especially in the case of complicated crystal structures. However, in simple crystal structures like the present, the evolution of the Raman modes of the ambient conditions rutile phase of ZnF_2 and the mode correlations[12,15] provide strong evidence that the space group of the high-pressure phase is the orthorhombic D_{2h}^{12} which corresponds to the $CaCl_2$-type structure.

The Grüneisen parameters γ_T for all five modes observed in the high-pressure phase of ZnF_2 are also given in Table I. In these gamma evaluations, we have used the $\partial\omega/\partial P$ slope and mode frequency ω_0 values at ~4.5 GPa (Fig. 3) and the ambient conditions value[25] for the bulk modulus B. Two gamma values are given for the A_g soft mode of the high-pressure phase at 4.5 and 6.8 GPa; the large difference between these values reflects the high degree of nonlinearity of this soft mode.

IV. CONCLUSIONS

All the spectral variations described above from both sets of data provide clear evidence that a phase transition takes place in ZnF_2 at about 4.5 GPa. Considering the phonon compatibility along with the way the phonons vary (transform) with pressure, and the number of Raman-active phonons observed in the high-pressure phase, we conclude that the transition is from rutile (D_{4h}^{14}) to $CaCl_2$-type (D_{2h}^{12}) structure. It appears that the transition is driven by the B_{1g} (A_g) Raman phonon of the rutile-type ($CaCl_2$-type) structure which displays *soft mode behavior* in the high-pressure phase. The linear dependence of ω^2 of the A_g part of this mode with pressure and the gradual increase in intensity of the B_{1g} (former A_{2g}, silent) with pressure in the high-pressure phase, suggests mean field behavior[3,11,12,15,31] and a second-order transition. It is known[12,32] that a transition is classified as *proper ferroelastic* or *pseudoproper ferroelastic* depending on whether the order parameter Q is represented by the transverse acoustic mode corresponding to the shear elastic constant $(C_{11}\text{-}C_{12})/2$ or directly by the B_{1g} Raman-active optical phonon (which, in any case, is coupled[3,12] to the above shear elastic constant and the corresponding acoustic mode), respectively. In the former case, the transition is accompanied by an elastic instability. There are no data of elastic constants of ZnF_2 up to P_c (the relevant study[29] is limited to about 1 GPa), but, in a broader concept, the phase transition can be assigned as a second-order ferroelastic one,

bearing in mind the crucial part the $B_{1g}(A_g)$ soft mode plays in the process.

Finally, it must be pointed out that ZnF_2 shows a similar behavior with pressure as the rutile-structured dioxides GeO_2 (Ref. 11) and SnO_2 (Ref. 12); this is more evident in the pressure dependence of the B_{1g} mode: like the dioxides, the frequency of this mode in ZnF_2 does not fall to zero at P_c and this is contrary to what mean field theory[31] predicts. It has been shown[12] that such a pressure dependence of the B_{1g} soft mode constitutes further evidence that the phase transition from rutile-to-$CaCl_2$ structure is ferroelastic.

ACKNOWLEDGMENTS

We would like to thank Dr. F. Wallrafen (University of Bonn, Germany) for kindly supplying a single crystal of ZnF_2 and Professor U. Pohl (Technical University of Berlin) for bringing us into contact with Dr. Wallrafen.

[1] P. S. Peercy and B. Morosin, Phys. Rev. B **7**, 2779 (1973).
[2] J. L. Sauvajol, R. Almairac, C. Benoit, and A. M. Bon, in *Lattice Dynamics*, edited by M. Balkanski (Flamarion, Paris, 1978), p. 199.
[3] D. J. Lockwood, R. S. Katiyar, and V. C. Y. So, Phys. Rev. B **28**, 1983 (1983).
[4] J. Giordano and J. L. Sauvajol, Phys. Status Solidi B **147**, 537 (1988).
[5] D. J. Lockwood and M. G. Cottam, J. Appl. Phys. **64**, 5876 (1988).
[6] A. Perakis, E. Sarantopoulou, Y. S. Raptis, and C. Raptis, Phys. Rev. B **59**, 775 (1999).
[7] M. Nicol and M. Y. Fong, J. Chem. Phys. **54**, 3167 (1971).
[8] L. Nagel and M. O'Keefe, Mater. Res. Bull. **6**, 1317 (1971).
[9] G. A. Samara and P. S. Peercy, Phys. Rev. B **7**, 1131 (1973).
[10] J. Pascual, J. Camassel, P. Merle, B. Gil, and H. Mathieu, Phys. Rev. B **24**, 2101 (1981).
[11] J. Haines, J. M. Leger, C. Chateau, R. Bini, and L. Ulivi, Phys. Rev. B **58**, R2909 (1998).
[12] H. Hellwig, A. F. Goncharov, E. Gregoryanz, H. K. Mao, and R. J. Hemley, Phys. Rev. B **67**, 174110 (2003).
[13] A. Perakis, Y. C. Boulmetis, and C. Raptis (unpublished).
[14] H. Barninghausen, W. Bossert, and B. Ancelment, Acta Crystallogr., Sect. A: Found. Crystallogr. **40**, C96 (1984).
[15] C. Raptis, R. L. McGreevy, and D. G. Seguier, Phys. Rev. B **39**, 7996 (1989).
[16] H.-G. Unruh, D. Muhlenberg, and C. Hahn, Z. Phys. B: Condens. Matter **86**, 133 (1992).
[17] H. Arashi, J. Phys. Chem. Solids **53**, 355 (1992).
[18] J. Haines, J. M. Leger, and O. Schulte, Science **271**, 629 (1996).
[19] L. Ming and M. H. Manghnana, Geophys. Res. Lett. **6**, 13 (1979).
[20] J. Haines and J. M. Leger, Phys. Rev. B **55**, 11 144 (1997).
[21] J. Haines, J. M. Leger, F. Gorelli, D. D. Klug, J. S. Tse, and Z. Q. Li, Phys. Rev. B **64**, 134110 (2001).
[22] Y. Tsuchida and T. Yagi, Nature (London) **340**, 218 (1989).
[23] K. J. Kingma, R. E. Cohen, R. J. Hemley, and H. K. Mao, Nature (London) **374**, 243 (1995).
[24] S. P. S. Porto, P. A. Fleury, and T. C. Damen, Phys. Rev. **154**, 522 (1967).
[25] D. Gerlich, S. Hart, and D. Whittal, Phys. Rev. B **29**, 2142 (1984).
[26] M. F. Striefler and G. R. Barsch, Phys. Status Solidi B **67**, 417 (1975).
[27] J. Pascual, J. Camassel, P. Merle, and H. Mathieu, J. Phys. Colloq. **42**, C6-719 (1981).
[28] A. S. Vinogradov, S. I. Fedoseenko, S. A. Krasnikov, A. B. Preobrajenski, V. N. Sivkov, D. V. Vyalikh, S. L. Molodtsov, V. K. Adamchuk, C. Laubschat, and G. Kaindl, Phys. Rev. B **71**, 045127 (2005).
[29] D. S. Rimai, Phys. Rev. B **16**, 2200 (1977).
[30] J. F. Nye, *Physical Properties of Crystals* (Clarendon Press, Oxford, 1985).
[31] J. F. Scott, Rev. Mod. Phys. **46**, 83 (1974).
[32] J. A. Valgoma, J. M. Perez-Mato, A. Garcia, K. Schwarz, and P. Blaha, Phys. Rev. B **65**, 134104 (2002).